Chinese Journal of
POLYMER SCIENCE

RESEARCH ARTICLE

https://doi.org/10.1007/s10118-026-3554-4
Chinese J. Polym. Sci.

Photostabilization of Poly(butylene adipate-*co*-terephthalate) (PBAT) Films with Hindered Amine Light Stabilizers: Performance Evaluation and Mechanistic Insights

Yang Wang[a], Wen-Qing He[a,b], Su-Nan Tian[c], Yue Wang[a], Run-Hao Bai[a], Aurore Richel[d], Qiu-Yun Liu[e], Jia-Lei Liu[a], Cai-Bin Li[f], He-Qing Cai[f], Zhi-Chao Zhen[g*], and Qi Liu[a*]

[a] *Key Laboratory of Prevention and Control of Residual Pollution in Agricultural Film, Ministry of Agriculture and Rural Affairs, Institute of Environment and Sustainable Development in Agriculture, Chinese Academy of Agricultural Sciences, Beijing 100081, China*
[b] *Institute of Western Agricultural, Chinese Academy of Agricultural Sciences, Changji 831100, China*
[c] *IMDEA Materials Institute, C/Eric Kandel, 2, 28906 Getafe, Madrid, Spain*
[d] *Laboratory of Biomass and Green Technologies, University of Liege, Gembloux 2 B-5030, Belgium*
[e] *The BioComposites Centre, Bangor University, Bangor LL57 2UW, UK*
[f] *Bijie Tobacco Company of Guizhou Province, Bijie 551700, China*
[g] *National Engineering Research Center of Engineering Plastics and Ecological Plastics Technical, Institute of Physics and Chemistry, Chinese Academy of Sciences, Beijing 100190, China*

Abstract The application of poly(butylene adipate-*co*-terephthalate) (PBAT) biodegradable plastics has long been constrained by insufficient light aging resistance. Hindered amine light stabilizers (HALSs), known as eco-friendly additives, can scavenge free radicals to enhance polymer durability. However, rough choices have resulted in wastage of resources and environmental pressure. Based on the application of plastic films as the background for use, this study systematically evaluates application effects of five HALSs. The films underwent accelerated aging for various durations and were further investigated by a combination of experiments and molecular simulation. Results showed that all HALSs mitigated PBAT light aging, with Chimassorb-944 (UV-944) and Tinuvin-770 (UV-770) performing the best for real applications. Quantum chemical calculation results showed that UV-944 had stronger anti migration ability. After 300 h of aging, films with UV-944 and UV-770 retained superior tensile strength and elongation at break in the transverse direction compared to neat PBAT films. Polymeric HALSs provided better long-term stability than small-molecule ones. Further spectra analysis indicated that stronger C—O bonds in HALS/PBAT composites correlated with improved photostability. This study offers valuable insights into improving weather resistance of PBAT biodegradable films and optimizing the real application of HALSs.

Keywords Poly(butylene adipate-*co*-terephthalate); Hindered amine light stabilizers; Accelerated aging; Light aging resistance; Mechanism

Citation: Wang, Y.; He, W. Q.; Tian, S. N.; Wang, Y.; Bai, R. H.; Richel, A.; Liu, Q. Y.; Liu, J. L.; Li, C. B.; Cai, H. Q.; Zhen, Z. C.; Liu, Q. Photostabilization of poly(butylene adipate-*co*-terephthalate) (PBAT) films with hindered amine light stabilizers: performance evaluation and mechanistic insights. *Chinese J. Polym. Sci*. https://doi.org/10.1007/s10118-026-3554-4

INTRODUCTION

Traditional plastic films are widely used in the fields such as commodity packaging and agricultural production due to their excellent comprehensive performance and low cost.[1–3] However, they, primarily made of polyethylene (PE), possess severe environmental challenges due to their very slow degradation. The amount of plastic residues in soil worldwide ranges from 1 kg/ha to 2700 kg/ha, while microplastic concentrations range from 0.01 mg/kg to 6.00×10^5 mg/kg.[4] Biodegradable plastic films have emerged as a promising, eco-friendly alternative that can replace traditional PE plastic films and reduce white pollution.[5] Among diverse biodegradable plastic films, poly(butylene adipate-*co*-terephthalate) (PBAT), a new type of aliphatic-aromatic polyester, offers great potential owing to its excellent performance and good biodegradability.[6,7] However, the biodegradable plastic films are usually limited by their weak light aging resistance and susceptibility to photodegradation.[8,9] When exposed to outdoor conditions, they are more vulnerable to weathering,[10] which deteriorates their performance and thus being unable to meet the needs of commercial and agricultural use. Therefore, improving the weather resistance of biodegradable plastic films is crucial for their widespread application and further reduction of environmental pressure.

Currently, the main strategies for improving the weather resistance of PBAT films involve blending modification and resin modification. Kijchavengkul *et al*. blended hydroxy-

* Corresponding authors, E-mail: zhenzc@mail.ipc.ac.cn (Z.C.Z.)
E-mail: liuqi@caas.cn (Q.L.)

Received September 12, 2025; Accepted January 16, 2026; Published online March 11, 2026

© Chinese Chemical Society
Institute of Chemistry, Chinese Academy of Sciences

toluene with PBAT to reduce the generation of free radicals during the film photo-oxidation process. They noted that the addition of carbon black helps absorb photon energy, thereby decreasing the intensity of reactions with the polymer and improving weather resistance.[8] Zhang *et al*. proposed enhancing weather resistance of films by blending PBAT and polylactide (PLA) using an chain extender and incorporating a light stabilizer to further extend its lifespan.[11] Marina *et al*. assessed the influence of the plasticizer polyethylene glycol on the compatibilization of PBAT and thermoplastic whey protein isolate blends, indirectly improving the film's weather resistance through this method.[12] Qiu *et al*. suggested that nano-polyhedral oligomeric silsesquioxane addition during PBAT/PLA film production for the production of high-performance biodegradable plastic packaging films.[13] Wang *et al*. used a styrene-methyl methacrylate-glycidyl methacrylate copolymer as a reactive compatibilizer in melt blending to induce ribbon-like PHBV lamellae in PBAT, enhancing mechanical and barrier properties.[14] Yan *et al*. synthesized PBAT by re condensing recycled PBT plastic with PBA using the polycondensation-coupling ring-opening polymerization method, and improved the properties of the newly generated polyester by adjusting the ratio.[15] Liu *et al*. proposed a strategy to incorporate lactide units into PBAT, aiming to enhance barrier performance and biodegradability.[16] In summary, the key to improving weatherability lies in preventing the photodegradation process within polyesters and slowing the changes in chemical composition and structures. To address this issue, light stabilizers are commonly used during the production of films to ensure enhanced weatherability during their application.[17]

Hindered amine light stabilizer (HALS), as free radical scavengers, are a class of organic amine compounds with steric hindrance effects that quenches singlet oxygen and capture radicals generated during polymer photolysis.[18] They have been proved to be one kind of the most effective light stabilizers.[19–23] HALS can slow down the further photoaging of materials by capturing and neutralizing the free radicals generated by photodegradation and simultaneously decomposing peroxides.[24] Cho *et al*. improved weather resistance by reducing the cross-linking density and curing rate of polyesters with the introduction of the benzotriazole-type UV absorber (Tinuvin 328), while adding the hindered amine light stabilizer (Tinuvin 292) simultaneously.[21] Davand *et al*. exposed high-density polyethylene (HDPE) samples containing phenolic antioxidants and different levels of HALS to ultraviolet radiation, compared the effects of different hindered amine light stabilizers, and proposed application recommendations.[22] Jiang *et al*. evaluated the effects of HALSs with different molecular structures on the UV resistance of HDPE.[23] Previous studies have predominantly focused on conventional polymers. However, comparative studies on their actual effects in biodegradable films, specifically PBAT, remains underexplored. Currently, a limited number of studies provide valuable insights for this. Wang *et al*. investigated the effects of blending PBAT, PLA, poly(propylene carbonate) (PPC), and HALSs on mechanical properties, thermal behavior, miscibility and light stability of plastic films, offering insight into performance optimization.[25] Patricia *et al*. examined the effects of various combinations of carbon black, HALSs, and vitamin E on the weather resistance of PBAT films.[20,26] Maisara *et al*. explores the transformative potential of protective additives (UV absorbers, light stabilizers, and anti-hydrolysis agents) in enhancing PBAT biocomposite's resilience.[27] Although current research emphasizes the effectiveness of HALS in enhancing the weather resistance of PBAT films, the differences in the effectiveness of different types of HALS under long-term outdoor exposure and scientific guidance for HALS use remain key knowledge gaps in promoting sustainable polymer engineering. Meanwhile, most past studies have focused on macroscopic performance characterization, lacking systematic analysis at the molecular level. Cross-scale cross-analysis can systematically reveal the dynamic mechanism of the interaction between different HALS molecular structures and the PBAT matrix, thereby providing a theoretical basis for designing customized HALS molecules with directional weather resistance improvement.

Herein, PBAT and HALS/PBAT blend samples containing five commonly used HALSs were prepared *via* extrusion blow molding. The films underwent artificial accelerated aging treatment for various durations and were investigated by a combination of experiments and molecular simulation. The research focused on analyzing the internal changes in the film that occurred during aging and comparing the mechanical properties with different types of HALSs over different aging times. The impact of different HALSs on the photostability of PBAT films was analyzed by combining molecular structural characteristics and spectral signatures. After eliminating the influence of objective factors, we found that the change in the content of C—O bonds during the aging process largely reflects the aging effect of TEMPO. This insight may provide a methodological basis for the rapid prediction of additive synthesis and the selection of composite film formulations. By combining molecular simulation with changes in film properties, the types of HALS with outstanding and long-lasting capabilities have been identified. This study offers valuable insights into improving weather resistance of PBAT biodegradable films and optimizing the application of HALSs.

EXPERIMENTAL

Materials

The selected HALS are Tinuvin-622, Chimassorb-119, Tinuvin-770, Chimassorb-944, Light Stablizer-783. Detailed information is presented in Fig. S1 (in the electronic supplementary information, ESI). Based on the numerical names of the HALS used, they were abbreviated and named as UV-622, UV-119, UV-770, UV-944, UV-783. Light stabilizers were all purchased from ANPEL Technology Company (Shanghai, China) and J&K Technology Company (Beijing, China). PBAT (Ecoworld®) was supplied by Shanxi Jinhui Zhaolong High Tech Co., Ltd. All polymers and reagents were dried before use.

Sample Preparation

The mass ratio of PBAT to the light stabilizers was maintained as 100/1. The components were thoroughly mixed and processed in a twin-screw extruder (LET-26-44, Labtech Engineering, Thailand) for melting and homogenization. The obtained samples were marked as 944/PBAT, 119/PBAT, 783/PBAT, 622/PBAT,

https://doi.org/10.1007/s10118-026-3554-4

and 770/PBAT based on the actual serial numbers of the HALS added. The extruder temperature zones were controlled between 175 and 185 °C, with a processing speed at 175 r/min. After extrusion, the blends were cooled and granulated using a pelletizer. The resin particles were subsequently processes into film using a single screw extrusion blown film machine, with a blowing expansion ratio of 2.5/1.0 and a temperature of 150 °C in all zones. Composite PBAT films with a thickness of 25.0±2.5 μm were produced by this method, including two types: those with HALS added and those without HALS added.

Accelerated Aging

The prepared films underwent accelerated aging in a xenon lamp aging chamber (BGD 860, Biuged, China). The accelerated aging conditions were designed with reference to the international standard ISO 4892-2:2013, which provides guidelines for exposing plastics to filtered xenon-arc light simulating solar radiation. In order to observe the aging process of the film in more detail, we intentionally reduced the aging intensity. The aging program involved 300 h of exposure at an intensity of 0.34 W/(m^2·nm), with the wavelength set at 340 nm. During the entire aging cycle, distilled water was sprayed at intervals of 120 min for 18 min to simulate environmental factors such as rainfall and humidity. Samples were sequentially aged, and at specific intervals (50, 100, 200, and 300 h), portions of the films were removed for subsequent analysis. The entire film aging process in this experiment was conducted using the xenon lamp aging chamber. Samples were stored in the dark and at low temperatures during transportation and the test preparation stage.

Characterizations

Scanning electron microscopy (SEM)

The morphology of all film samples, both before and after aging, was examined using SEM. The dried samples were mounted on a carbon conductive tape and coated with a 10 nm platinum/palladium (80/20, *W/W*) alloy using a sputter coater (208HR, Cressington Scientific Instruments Ltd., Watford, England). The films were then analyzed using a scanning electron microscope (SU8010, Hitachi, Japan) operating at an acceleration voltage of 20 kV. IMAGE J was used to analyze the surface roughness of SEM images.

Fourier transform infrared (FTIR)

FTIR (Lumos, Bruker, Germany) was used to record the spectral range from 4000 cm^{-1} to 600 cm^{-1} with a resolution of 4 cm^{-1} for each film. The measurements were conducted in the attenuated total reflectance (ATR) mode to obtain fully reflected infrared spectrum. The carbonyl index (CI) was utilized to quantify the transformation of the carbonyl group (C=O) in the samples, which was calculated using the following equation:

$$CI = \frac{A_{C=O}}{A_{ref}} \quad (1)$$

where $A_{C=O}$ represents the band area of the C=O bond from 1766 cm^{-1} to 1677 cm^{-1} and A_{ref} denotes the band area of the C—H bond from 755 cm^{-1} to 697 cm^{-1} as the reference.

Gel permeation chromatography (GPC)

The molar mass of each film was determined using GPC (KF804L, Shodex, Japan). Each film sample (10 mg) was dissolved in 3 mL of tetrahydrofuran (THF) at room temperature, followed by centrifugation and filtration through a 0.2 μm polytetrafluoroethylene (PTFE) filter. A volume of 100 μL of the prepared solution was injected into the GPC system for testing. The solvent used was THF, with a mobile-phase flow rate of 1 mL/min and a temperature of 40 °C. The standard sample was a narrow-distributed polystyrene (PS) standard. The size of the gel permeation chromatographic column was 7.8 × 300 mm, and the filler consisted of a gel of styrene and vinyl benzene. The polymer density index (PDI) was calculated using the following equation:

$$PDI = \frac{M_w}{M_n} \quad (2)$$

where M_w denotes the weight-average molecular weight and M_n represents the number-average molecular weight.

Differential scanning calorimetry (DSC)

The melting and crystallization behaviors of the film samples were analyzed using DSC (DSC250, TA, USA). Each sample, weighing 3–7 mg, underwent a three-step procedure involving heating, cooling, and heating ramps in a N_2 atmosphere. Initially, the samples were heated from 25 °C to 200 °C and melted for 2 min to eliminate the heat history. They were then cooled from 200 °C to 25 °C and maintained at 25 °C for 3 min to record their crystallization behavior. Finally, the samples were heated again to 200 °C to record their melting behavior. The heating and cooling rates for the experiment were both set at 10 °C/min. The degree of crystallinity of the samples (X_c) was calculated as follows:

$$X_c\ (\%) = \frac{\Delta H_f}{\Delta H_m^\circ \times (1 - w)} \times 100\% \quad (3)$$

where ΔH_f is enthalpy of fusion, ΔH_m° is enthalpy of fusion of 100% crystalline PBAT (114 J/g),[28] and w is mass fraction of additives.

Thickness

According to ISO 4593:1993,[29] the thickness of films was tested using a thickness tester (MahrGmbH-Esslingen C1200, Mahr Company, Germany) (accuracy: 0.0001 mm). For the transverse sample, the point of measurement was determined as follows: for a sample width $w \leq 800$ mm, 10 points were measured; for 800 mm$<w<$1500 mm, 15 points were measured; and for $w \geq$ 1500 mm, 20 points were measured. The average value of all points was taken as the sample thickness, which was 22.5±2.0 μm.

Tensile test

A universal tensile testing machine (XLW, Labthink, China) was used to test the maximum tensile strength and elongation at break in the machine direction (MD) and transverse direction (TD), respectively, of the samples. In the tensile testing experiment, the plastic film was cut into rectangular samples measuring 10 mm in width and 80 mm in length, with a clamping distance of 50 mm and a stretching speed of 250 mm/min. Each sample was tested at least six times, and the final result was taken as the average.

Quantum chemical calculation

All electronic-structure calculations were performed with ORCA. Geometry optimizations and transition-state (TS) searches used the B97-3c functional with the def2-TZVP basis set. Stationary points were confirmed by harmonic vibrational frequency analysis at the same level, and zero-point energy (ZPE) corrections

were obtained from the Hessian. High-accuracy single-point energies were computed at the normal DLPNO-CCSD(T)/def2-TZVPP level with the RIJCOSX approximation and the def2-TZVP/C auxiliary basis set.

Molecular dynamics simulation

Coarse-grained molecular dynamics (M) simulations were performed in BIOVIA Materials Studio using the Mesocite module. Atomistic PBAT (M_n≈4.0×10^4 g/mol) and the HALS molecules were mapped to the C2 particle model; each coarse-grained bead was assigned a standard mass of 72 g/mol as defined by the force field. Periodic simulation boxes were constructed at a fixed mass density of 1.2 g/cm^3, each containing two PBAT chains and one HALS molecule (UV-770 or UV-944). After energy minimization and equilibration, trajectories were propagated in the canonical (NVT) ensemble at 298 K using Mesocite defaults appropriate for the C2 model.

RESULTS AND DISCUSSION

Microscopic Morphology Changes

The aging of polymers typically begins on their surface, where defects can lead to void formation, resulting in an increased contact area with oxygen and further degradation of the material.[30] Therefore, it is essential to observe the changes in the microstructure of PBAT films. Fig. 1 shows a comparison of the microstructure of PBAT films with those of PBAT samples containing different HALS additions after aging for 0 and 300 h. At 0 h of aging, a difference in the surface smoothness was observed, attributed to the incomplete mixing of the PBAT masterbatch and HALS powder during the melt blow molding process. After aging for 300 h, the PBAT film surface became very rough, resulting in extensive porosity and severe cross-linking phenomena. In contrast, the surface of 119/PBAT film also became rough, while the other PBAT samples treated with HALS exhibited less pronounced micro-cracking and void. This result is similar to the trend of microstructure changes in PBAT films in the work of Morales *et al*.[26] We also conducted grayscale quantitative analysis on the images of the samples aged for 0 and 300 h, and the results are summarized in Table S1 (in ESI). The data indicated that after 300 h of aging, the arithmetic mean deviation (Ra) of the contour of the PBAT film increased by 1304%, while those of the samples with HALS addition increased by 124.9%–380.4%. Although none of the samples displays considerable degradation, the incorporation of HALS significantly slowed the rate of surface roughening in PBAT, indicating that HALSs can effectively mitigate the overall aging process of PBAT.

Spectral characterization

Fig. 2 shows the FTIR spectra of all samples after aging for 0 and 300 h, and highlights two types of functional groups. The first type is the stretching vibration bands of C=O groups related to molecular chain breakage during PBAT photoaging, which appear around 1766–1677 cm^{-1}. The bands are attributed to result from the cleavage of ester bonds (R—COO—R') in the PBAT molecular chains during photoaging. The stretching vibration peak of alcohol C—O groups, observed around 1300–1000 cm^{-1}, is linked to the impact of HALS on the photoaging of PBAT. The quantitative analysis results of the CI are presented in Fig. 2(f). The data indicate that all aged samples showed an increasing CI trend, with the CI ranging from initial to significantly higher values with prolonged exposure. This suggests that PBAT undergoes molecular chain cleavage during photodegradation, resulting in the formation of short-chain carboxylic acids, as supported by previous research.[31,32]

PBAT typically produces acyl, hydroxyl, hydrocarbon, and alkyl free radicals during photodegradation,[33] leading to chain initiation, chain growth, chain branching, and chain termination, where molecular chains may cross-link to form longer chains or break to create shorter chains. When HALSs

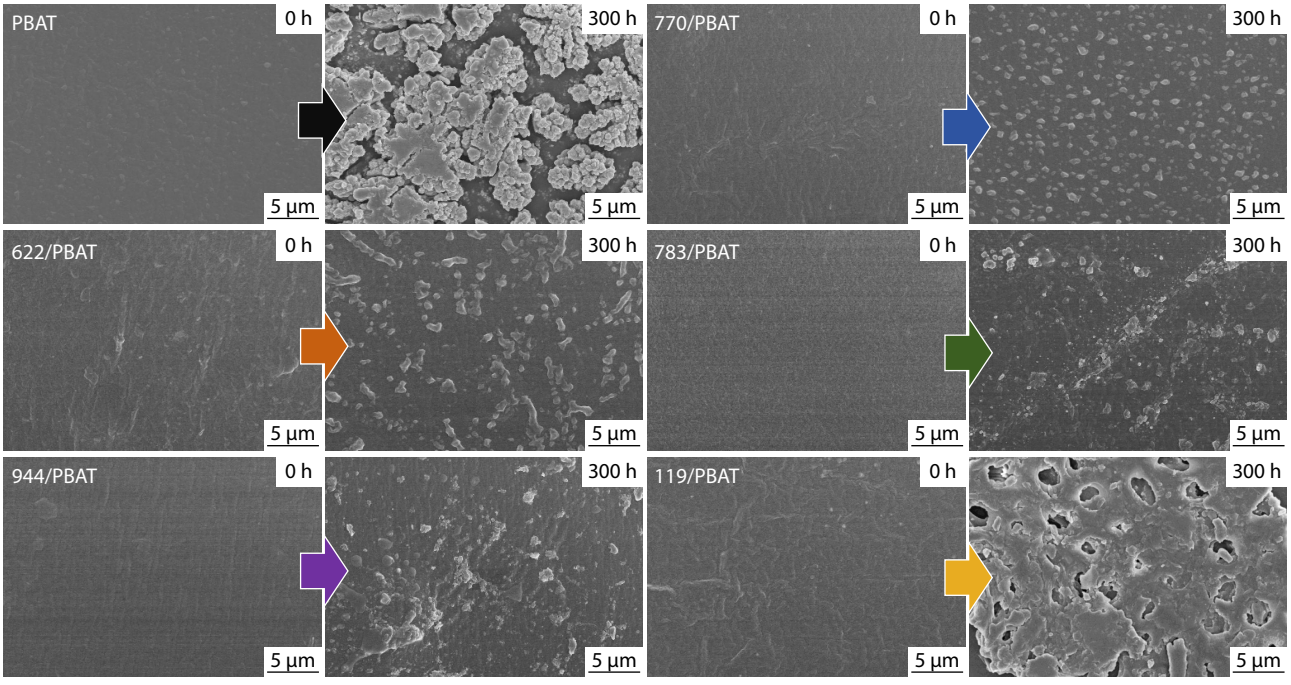

Fig. 1 SEM images of PBAT film and PBAT with different HALSs add after aging for 0 and 300 h and magnified 5000 times.

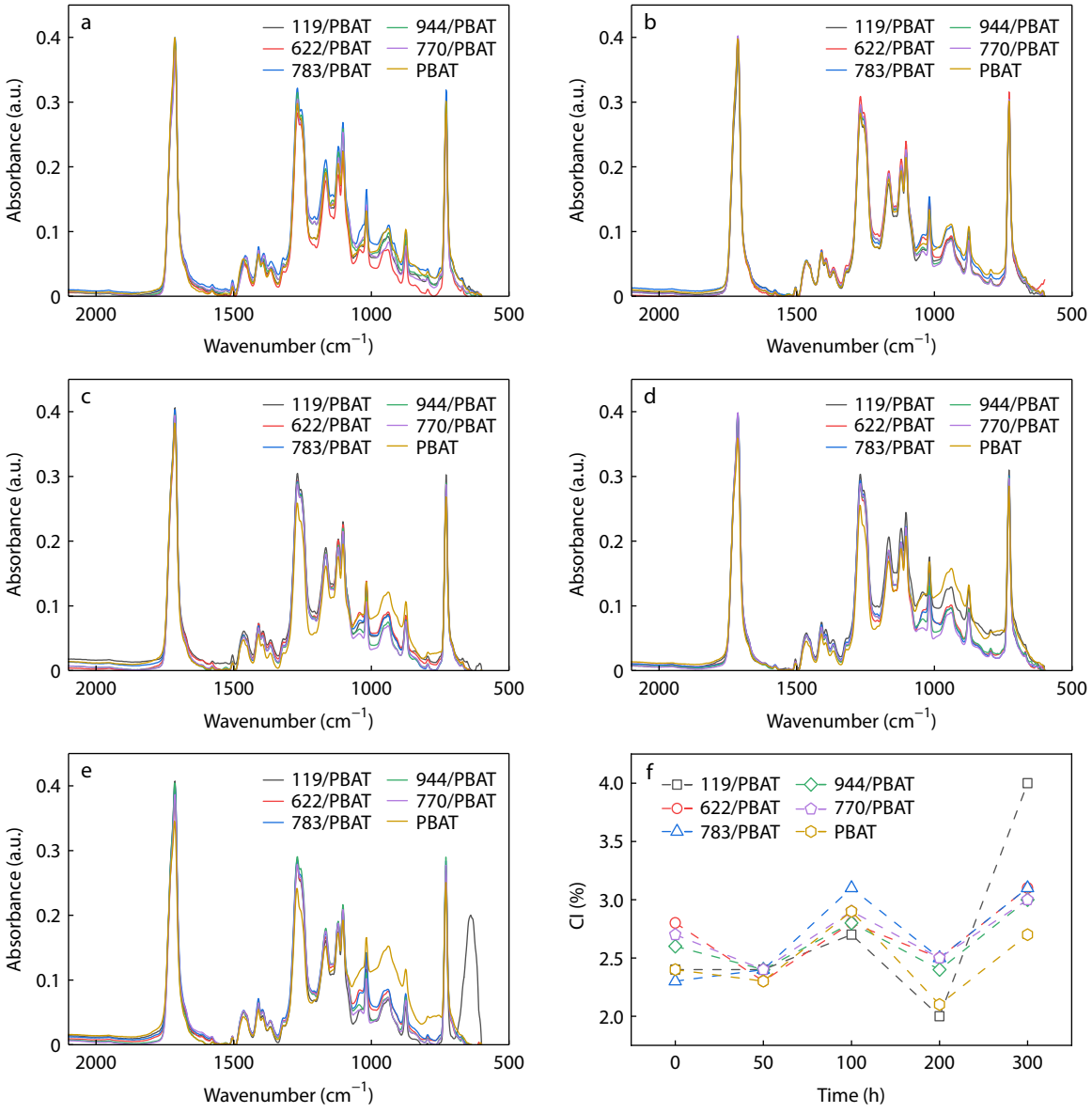

Fig. 2 FTIR spectra and analysis of samples after aging for (a) 0, (b) 50, (c) 100, (d) 200 and (e) 300 h, (f) CI calculation results.

are oxidized, their primary functional group, 2,2,6,6-tetramethylpiperidin-1-oxyl (TEMPO), captures free radicals.[34] This process directly enables the transition from the chain initiation phase to the chain termination phase. Upon capturing alkyl free radicals, TEMPO effectively reduces the number of C—O bonds formed during the four-step reaction, leading to a decrease in the C—O absorption band. Previous studies have shown that TEMPO reacts with polymer alkyl radicals to form alkoxylamines, which is a rapid and exothermic reaction that directly involves the formation of C—O bonds and is the initial step of the "Denisov cycle". The literature emphasizes that this reaction is "essentially barrierless", indicating that the formation of C—O bonds is kinetically highly favorable. Secondly, in the subsequent reactions, when alkoxylamine reacts with peroxyl radicals, TEMPO is ultimately regenerated through intermediates and ketone and alcohol products are formed. This process involves the recombination of C—O bonds, and literature calculations show that its free energy barrier is relatively low, further indicating that the participation of C—O bonds is at the core of the cycle.[34] Therefore, the variation of the C—O absorption band in the range of 1000–1300 cm^{-1} has the potential to evaluate HALS in scavenging free radicals, in other words, its anti-photoaging ability.

We calculated the area of the C—O absorption band in the range of 1000 cm^{-1} to 1300 cm^{-1}. The analysis of the relative number of C—O bonds was achieved by calculating the ratio of the area of the C—O absorption band to the C—H absorption band in the range of 697–755 cm^{-1}, and the result are shown in Table 1. It is worth noting that, apart from the non-amine-based HALS in 119/PBAT and 622/PBAT, all other HALS samples used in this study contain amine structures.

During the mixing process, amine groups react with the ester bonds present in PBAT films, leading to the formation of

Table 1 Calculation results of C—O bond number.

Sample	Aging time (h)	Area of the C—O absorption band	Area of the C—H absorption band	C—O bond number	Change value compared to the PBAT film (%)
PBAT	0	41.8	6.1	6.9	–
119/PBAT		41.2	5.8	7.1	3.6
622/PBAT		38.4	4.9	7.8	13.0
783/PBAT		48.7	6.2	7.9	12.4
944/PBAT		45.4	5.3	8.5	24.0
770/PBAT		45.0	5.4	8.9	29.4
PBAT	300	37.6	5.1	7.4	–
119/PBAT		34.4	3.8	9.1	22.7
622/PBAT		38.8	4.7	8.3	12.3
783/PBAT		39.6	4.9	8.2	8.8
944/PBAT		38.2	4.9	7.8	4.9
770/PBAT		34.1	4.7	7.3	−1.3

amide bonds and consequently increasing the number of C—O bonds. The occurrence of this reaction is closely related to the degree of dispersion of HALS and the positioning of the amine groups within the HALS structure. Among these, HALS with smaller molecular structures exhibit higher dispersibility during the processing stage. Additionally, the amine groups located on the outer regions of their structures are more likely to interact with the PBAT molecular chains, thereby accelerating the reaction rate. We can approximately conclude that the order of the number of C—O bonds in the samples is as follows: (1) Small molecules with two amine groups (UV-770); (2) Large molecules with two amine groups (UV-944); (3) Mixtures of large molecules containing amine groups (UV-783); (4) Molecules with ester groups but no amine groups (UV-622); (5) Molecules with neither ester groups nor amine groups (UV-119). This inference aligns with the calculated sequence of C—O bond relative content in the sample films after aging for 0 h.

As previously analyzed, with increasing aging time, the most efficient HALS for capturing free radicals will lead to a more pronounced decrease in the relative quantity of C—O bonds. After 300 h of aging, the relative number of C—O bonds decreased most significantly in 770/PBAT, followed by 944/PBAT, 783/PBAT, 622/PBAT, and 119/PBAT. The results demonstrate that the HALS employed in 770/PBAT and 944/PBAT offer notable benefits in scavenging free radicals produced by PBAT during photoaging. The calculated C—O bond results correspond to the elongation at break retention results of the relevant samples after aging for 300 h.

Molecular weight

Experimental results indicated that with increasing aging time, M_n of all samples decreased, while M_w initially increased and then decreased. The change in M_n indicates that all samples underwent the Norrish I reaction, leading to chain cleavage during the accelerated aging process.[8] Specific data is provided in Table S2 (in ESI). The temporal variation in M_w for all is presented in Fig. 3. Most high-molecular-weight peaks of the samples exhibited an initial increase followed by a decrease over time. This M_w trend is attributed to the accumulation of macromolecular substances formed *via* the recombination of broken molecular chains during the early stage of photolysis, resulting in an increase in M_w.[35] In the later stage of photolysis, extensive chain cleavage degradation of PBAT long chains produces numerous inorganic small-molecule substances, leading to a decrease in M_w. After aging for 300 h, the M_w of the sample containing HALSs was higher than that of the PBAT film, suggesting a greater degree of cross-linking and/or branching.[20]

A smaller PDI indicates a more uniform molecular weight distribution within a film. The calculated PDI values for the films at various aging time are presented in Table 2. After long-term aging, maintaining high M_n and M_w while achieving low PDI indicates effective alleviation of molecular chain breakage. After 300 h of aging, M_n was obtained in descending order of 944/PBAT, 119/PBAT, 783/PBAT, 622/PBAT, 770/PBAT, and PBAT. M_w was obtained in descending order of 944/PBAT, 119/PBAT, 770/PBAT, 783/PBAT, 622/PBAT, and PBAT. The PDI values from smallest to largest were 944/PBAT, 783/PBAT, 622/PBAT, 119/PBAT, PBAT, and 770/PBAT. Consequently, the 944/PBAT films demonstrated significant advantages in reducing PBAT degradation and managing the cross-linking of degradation products during prolonged aging. It is noteworthy that UV-770 still exhibits excellent control over molecular chain degradation behavior after 200 h of aging. However, a significant amount of low-molecular-weight products can be observed after 300 h of aging. Based on the molecular simulation results of the HALS samples, we conclude that UV-770 shows a notable limitation in its effective duration. This phenomenon may be attributed to the substantial leaching of small-molecule HALS during the later stages of degradation, thereby preventing it from continuously exerting its functional effects.

Thermal behavior

The thermal performance test results are shown in Fig. 4. As the aging time increases, the T_m of PBAT films decreases, which is attributed to molecular chain scission and subsequent reduction in crystal dimensions within the film during photo-aging processes.[36] In contrast, the incorporation of HALS induced varying degrees of T_m elevation in PBAT films. This elevation suggests that HALS additives effectively retard the chain scission of PBAT macromolecules, thereby preserving the integrity of the crystalline structure.

The addition of HALS also influenced the crystallization behavior of PBAT. The heterogeneous nucleation effect induced by HALS in the PBAT matrix resulted in increased T_c and T_m,[37,38] As evidenced by narrower crystallization exotherms and lower PDI observed after aging. The enhanced nucleation effect promotes the formation of more stable and uniform crystalline structures. However, the 770/PBAT blend ex-

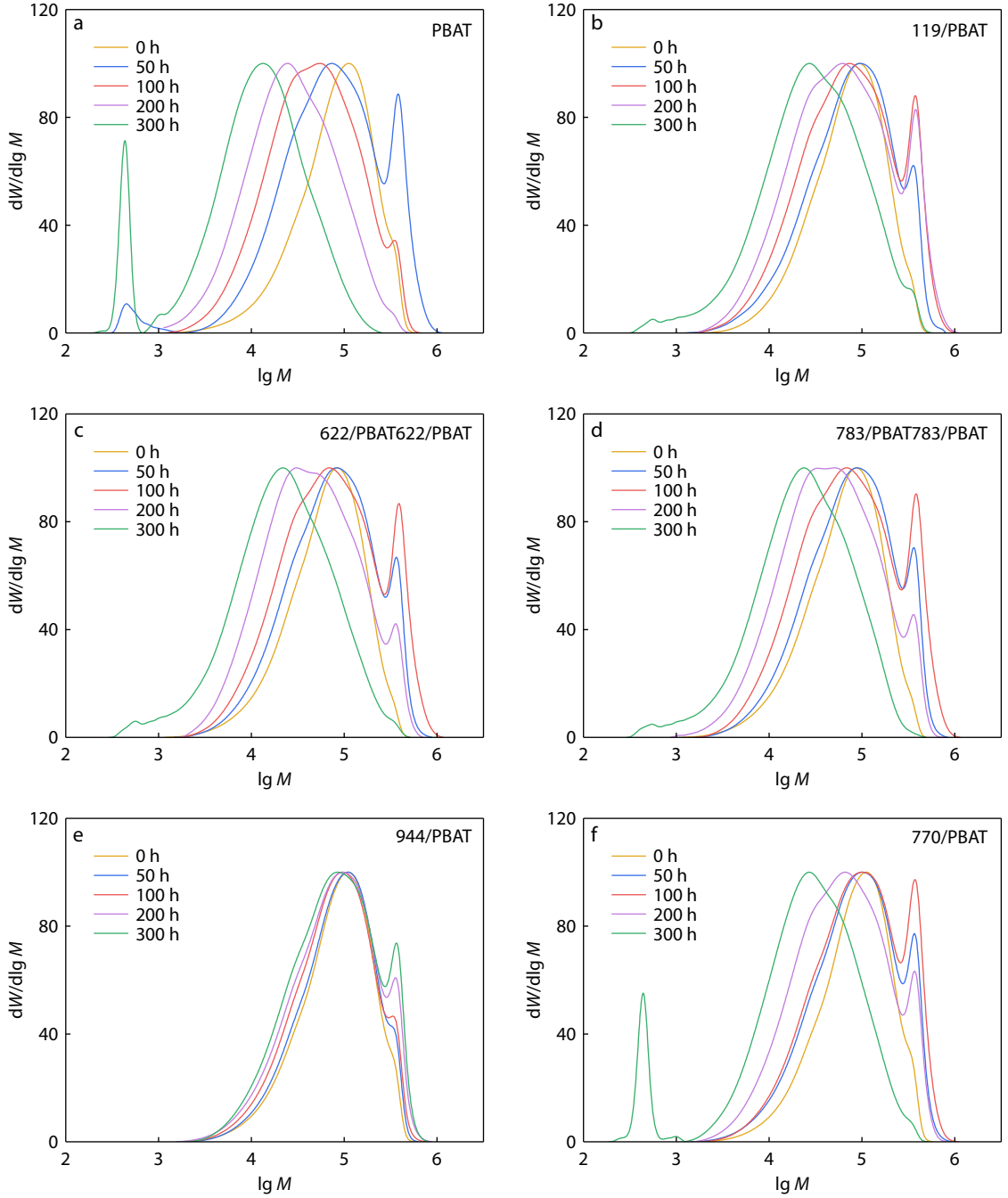

Fig. 3 GPC analysis of (a) PBAT, (b) 119/PBAT, (c) 622/PBAT, (d) 783/PBAT, (e) 944/PBAT, and (f) 770/PBAT.

Table 2 Calculation results of PDI of films under various aging durations.

Time (h)	PDI					
	PBAT	119/PBAT	622/PBAT	783/PBAT	944/PBAT	770/PBAT
0	2.4	2.2	2.3	2.4	2.2	2.2
50	3.3	3.0	2.1	3.0	2.3	2.9
100	3.1	3.5	3.7	3.8	2.5	3.1
200	3.1	4.0	3.4	3.7	2.8	3.3
300	6.3	4.9	4.6	4.2	2.9	9.8

hibits a T_m similar to that of neat PBAT but a lower T_c. As previously analyzed, the small-molecular-weight HALS does not effectively enhance the ordered arrangement of PBAT molecular chains. Instead, it increases the mobility of the molecular chains, making the recrystallization process more facile. This observation is consistent with the superior retention of elon-

https://doi.org/10.1007/s10118-026-3554-4

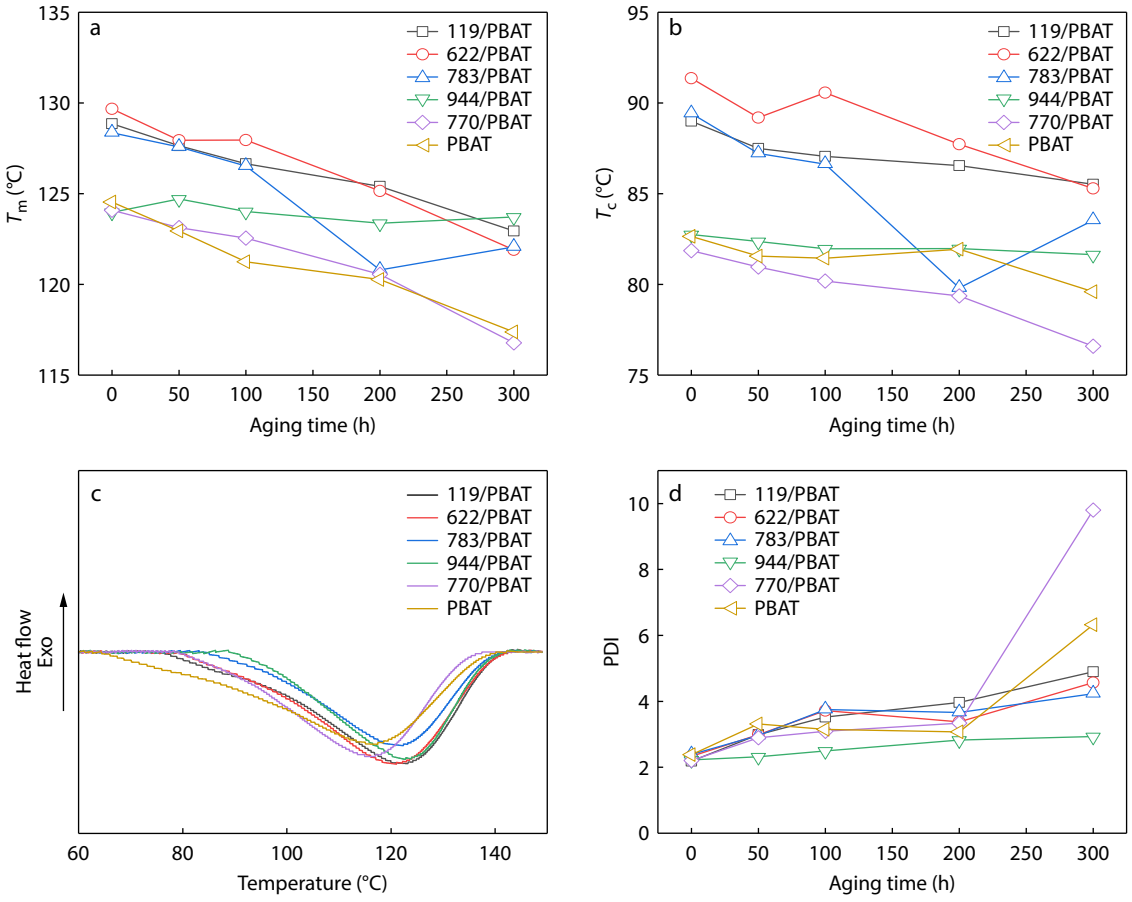

Fig. 4 Thermal performance characterization results: (a) T_m, (b) T_c, (c) heat absorb curve chart of the samples after 300 h of aging, (d) PDI changes with time.

Table 3 Calculation results of X_c (%) of films under various aging durations.

Time (h)	X_c (%)					
	PBAT	119/PBAT	622/PBAT	783/PBAT	944/PBAT	770/PBAT
0	7.1	6.4	6.3	6.4	6.2	6.0
50	6.1	6.2	6.5	6.7	7.0	6.3
100	6.5	6.5	6.1	6.7	7.2	7.3
200	6.4	6.2	6.4	7.9	6.9	6.3
300	6.4	6.3	6.0	4.9	6.6	6.1

gation at break, as observed experimentally.

A higher degree of crosslinking leads to the appearance of wider melting peaks,[39,40] and it appears from the results that the addition of HALS also slows down the formation of crosslinking. This part of the results corresponds to the earlier appearance of higher molecular weight peaks in PBAT in the molecular weight change curve graph. PBAT undergoes a complex photodegradation, leading to chain breakage. If HALSs are not involved, low-molecular-weight substances are usually produced in the later stage of degradation.[35] In the early stage of degradation, when the production of low-molecular-weight substances is low, cross-linking will largely only produce substances with larger molecular weight, resulting in a sudden increase in the signal intensity of high-molecular-weight in Fig. S2 (in ESI).

After 300 h of aging, the X_c of the samples, in descending order were as follows: 944/PBAT, PBAT, 119/PBAT, 770/PBAT, 622/PBAT, and 783/PBAT (Table 3). The increase in X_c in case of 944/PBAT may be due to their role in enhancing the internal crystal structure of PBAT, thereby promoting crystallization, but higher crystallinity is not conducive to maintaining elongation at break. In contrast, the reduced X_c in PBAT with HALS was attributed to these HALSs hindering molecular chain rearrangement, reducing the number of chains involved in crystallization, thereby obstructing enhancement in crystallization.[41] Based on the changes in molecular weight and thermal properties, results indicate that that 944/PBAT has a significant advantage in slowing down the breakage of molecular chains compared to the other four groups of HALS added PBAT. However, based on the final mechanical performance test results, even though the HALS used in 944/PBAT resulted in higher crystallinity of the film, slowing down the

breakage of molecular chains seems to be more effective in maintaining high mechanical properties of the film.

Molecular behavior

Based on the size of the group attached to the tetramethylpiperidine in TEMPO, the selected HALSs can be classified into two categories. The reaction processes of UV-770 and UV-944 are categorized as "Pathway-1", while those of UV-119, UV-622, and UV-783 are categorized as "Pathway-2". The reaction mechanisms and visualization results are shown in Fig. 5(a). To further clarify their relative reactivities, we conducted molecular dynamics simulation and quantum chemical analysis, and the results are presented in Figs. 5(b) and 5(c). Quantum chemical calculations revealed that the free energy barrier of Pathway-1 is only 70.88 kJ/mol, whereas that of Pathway-2 is 212.31 kJ/mol. Evidently, Pathway-1 exhibits a significant reactivity advantage.

The high efficiency of UV-770 and UV-944 in radical scavenging can be explained from the perspective of local chemical reactions. The main reason lies in the fact that this process only involves hydrogen atom transfer without steric hindrance, making it simpler compared to Pathway-2. For UV-770 and UV-944, even with identical active centers, quantifying molecular anti-migration capability is essential for practical applications. Results demonstrated that UV-944 exhibited significantly lower mean square displacement (MSD) values compared to UV-770, indicating superior molecular stability against migration. Through Einstein's equation analysis of MSD-time profiles, the diffusion coefficients were derived and plotted against molecular weights. The comparative analysis revealed that UV-944 possessed a lower diffusion coefficient than UV-770, while simultaneously exhibiting a higher molecular weight. Obviously, the

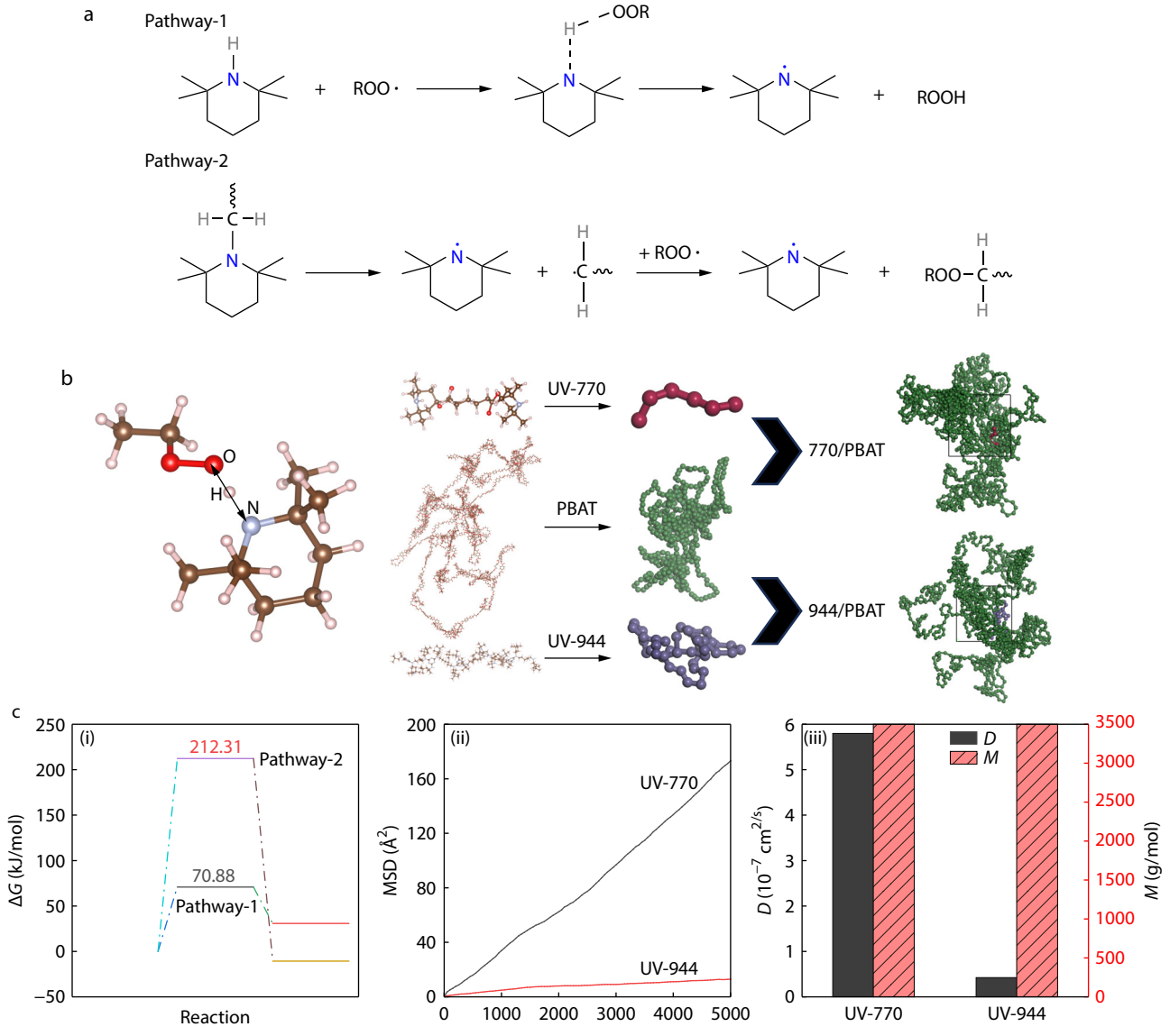

Fig. 5 Molecular behavior analysis: (a) reaction pathways of two types of TEMPO; (b) molecular dynamics simulation results; (c) quantum chemical and diffusion calculations, including (i) calculated free energy barriers of the two main reaction pathways, (ii) mean square displacement (MSD) as a function of time, and (iii) comparison of diffusion coefficient (*D*) with relative molecular weight (*M*) of the two HALS molecules.

https://doi.org/10.1007/s10118-026-3554-4

self-immobilization characteristics of high molecular weight HALS is the direct cause of the decreased mobility of their centers and the inhibition of migration losses. Therefore, it can be concluded that UV-944 demonstrates superior anti-migration capability compared to UV-770 among HALS with comparable activity advantages, exhibiting significant advantages for the sustained performance of polymer films.

Tensile properties

Compared to other application scenarios, the mechanical properties of thin films have special requirements in agricultural applications, a high machine direction (MD) maximum tensile strength is crucial for ensuring the film's integrity during the mechanized covering process, where higher tear resistance is often necessary. However, excessively higher MD elongation at break is unfavorable as this can lead to misalignment between punched holes and seeding positions, reducing crop germination rates due to seedlings being unable to survive after emergence. During crop growth, especially in the later stages, maintaining high MD and transverse (TD) elongation at break is essential for the film's elasticity and durability, improving its functionality in retaining warmth and moisture as well as controlling weed.

The mechanical performance test results are presented in Fig. 6. After 0 h of xenon lamp aging, only the MD maximum tensile strength of the 783/PBAT and 770/PBAT samples increased by 26% and 20%, respectively, compared to the PBAT film. All the samples did not show significant enhancement in TD elongation at break, possibly because the introduction of additives into the polymer created a complex multiphase system, affecting film's original performance either positively or negatively.[35,41] After 50 h of aging, the 944/PBAT and 770/PBAT samples showed notable improvements in MD maximum tensile strength, increasing by 37% and 29%, respectively, compared to the PBAT film. All samples demonstrated significantly enhanced TD elongation at break under the same conditions. After 100 h, the five films with added HALSs showed considerable improvements in both MD maximum tensile strength and TD elongation at break. Notably, the 944/PBAT sample displayed the most pronounced enhancement in TD elongation at break, with a remarkable 39% increase over that of the PBAT film. Furthermore, after 200 h, the PBAT film exhibited a sharp 92% decrease in TD elongation at break, indicating a complete loss of this attribute. In contrast, the 944/PBAT, 119/PBAT, and 770/PBAT films maintained significant TD elongation at break values of 364%, 252%, and 214%, respectively, demonstrating their improved stability under aging conditions. After 300 h, the PBAT film and the 119/PBAT, 622/PBAT, and 783/PBAT samples experienced >90% reductions in TD elongation at break. However, the 944/PBAT and 770/PBAT samples retained impressive elongation at break values of 427% and 324%, respectively. These results highlight the superior performance of both

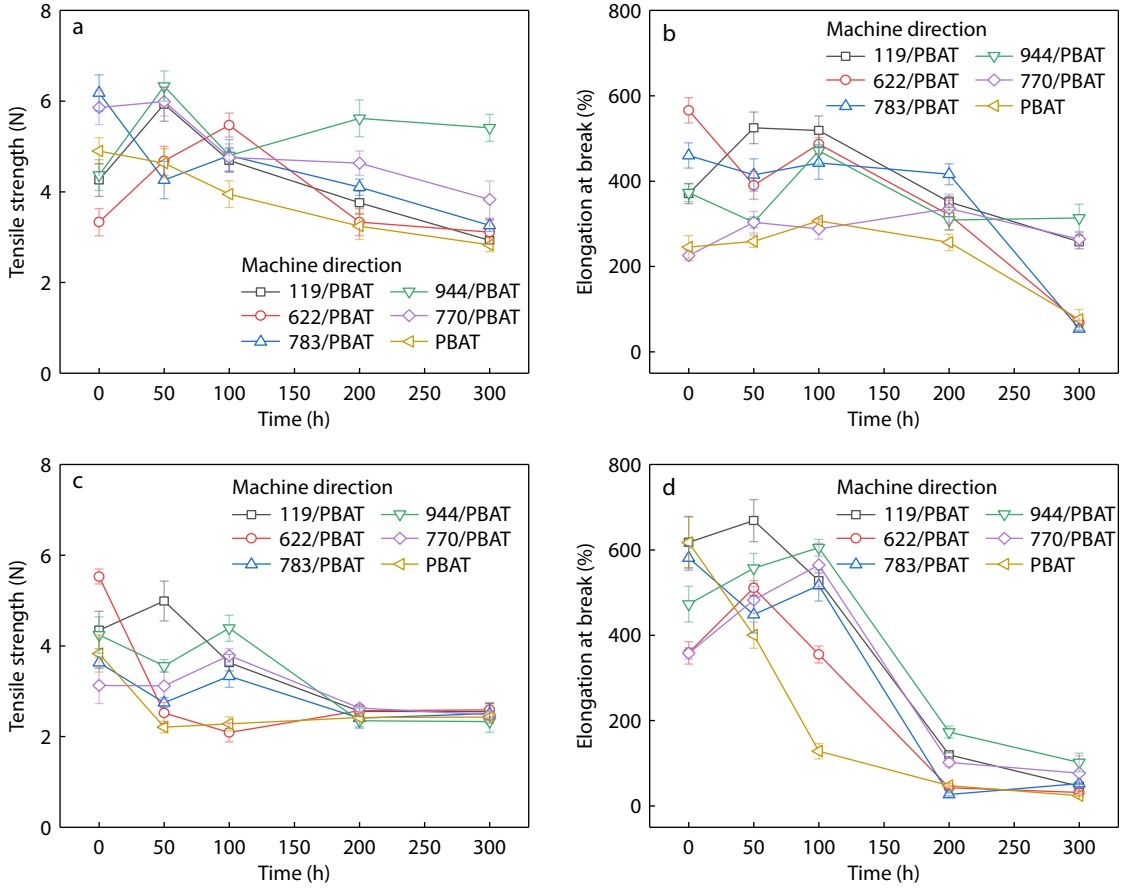

Fig. 6 Changes in mechanical properties of PBAT film and PBAT film with HALS added after aging: (a) tensile strength in MD, (b) elongation at break in MD, (c) tensile strength in TD, and (d) elongation at break in TD.

https://doi.org/10.1007/s10118-026-3554-4

944/PBAT and 770/PBAT in terms of tensile strength and TD elongation at break, even after prolonged aging, making them more durable than PBAT films.

CONCLUSIONS

This study investigated the differential effects of different HALS on the photostability and mechanical properties of PBAT biodegradable films through characterization and mechanical assessments. The specific HALS structure has a significant impact on its application activity and long-term effectiveness. Infrared characterization, molecular simulation, and quantum chemical calculations provide clear evidence, and mechanical performance testing further verifies these findings. UV-944 and UV-770 have been found to significantly mitigate the degradation process of PBAT, with UV-944 exhibiting particularly significant effects due to its chemical activity and anti-migration ability. Notably, PBAT films treated with UV-944 and UV-770 maintained TD elongation at break values of 21.5% and 21.6% compared to the original film, respectively, even after 300 h of aging. This indicates that the application of these HALSs in PBAT still has sustainable research value. This study offers valuable insights into improving weather resistance of PBAT biodegradable films and optimizing the application of HALSs. Most importantly, this study not only verified the macroscopic protection effect of HALSs but also revealed through simulation methods the regulatory mechanism of anti-migration on long-term performance, providing a new paradigm for the rational selection of HALSs.

Conflict of Interests

The authors declare no interest conflict.

Data Availability Statement

The data that support the findings of this study are available from the corresponding author upon reasonable request.

ACKNOWLEDGMENTS

This work was financially supported by the Key Research and Development Task Project of Xinjiang Uygur Autonomous Region (No. 2022B02033), the National Natural Science Foundation of China (Nos. 42211530566 and 42311530066), the NSFC-FNRS Joint Program BIOAGRIFILM (No. FNRS PINT-BILAT-M 2022), the Science and Technology Project of Bijie Tobacco Company of Guizhou Province (No. 2022520500240192) and the Agricultural Science and Technology Innovation Program (ASTIP). Special thanks to Xiangze Meng (mxz24@mails.tsinghua.edu.cn) from the Department of Chemical Engineering at Tsinghua University for his support in the quantum chemical calculation and molecular dynamics simulation work presented in this article.

REFERENCES

1 Tian, S.; Cao, X.; Luo, K.; Lin, Y.; Wang, W.; Xu, J.; Guo, B. Effects of nonhydroxyl oxygen heteroatoms in diethylene glycols on the properties of 2,5-furandicarboxylic acid-based polyesters. *Biomacromolecules* **2021**, *22*, 4823–4832.
2 Tian, S.; Du, Y.; Wang, P.; Chen, T.; Xu, J.; Yu, H.; Guo, B. Effects of different isomers of thiophenedicarboxylic acids on the synthesis and properties of thiophene-based sustainable polyesters. *ACS Sustainable Chem. Eng.* **2023**, *11*, 6652–6664.
3 Tian, S.; Shi, K.; Xu, J.; Guo, B. Synthesis and structure–property relationships of novel high molecular weight fully biobased 2,5-thiophenedicarboxylic acid-based polyesters. *Biomacromolecules* **2023**, *24*, 2998–3008.
4 Zhang, J.; Ren, S.; Xu, W.; Liang, C.; Li, J.; Zhang, H.; Li, Y.; Liu, X.; Jones, D. L.; Chadwick, D. R.; Zhang, F.; Wang, K. Effects of plastic residues and microplastics on soil ecosystems: a global meta-analysis. *J. Hazard. Mater*. **2022**, *435*, 129065.
5 Sander, M. Biodegradation of polymeric mulch films in agricultural soils: concepts, knowledge gaps, and future research directions. *Environ. Sci. Technol.* **2019**, *53*, 2304–2315.
6 Jiao, J; Zeng, X; Huang X. An overview on synthesis, propertiesand applications of poly(butylene-adipate-*co*-terephthalate) – PBAT. Advanced industrial and engineering. *Polym. Res.* **2022**, *3*, 19–26.
7 Nelson, T. F.; Baumgartner, R.; Jaggi, M.; Bernasconi, S. M.; Battagliarin, G.; Sinkel, C.; Künkel, A.; Kohler, H. E.; Mcneill, K.; Sander, M. Biodegradation of synthetic aliphatic-aromatic polyesters in soils: linking chemical structure to biodegradability. *Environ. Sci. Technol.* **2025**, *59*, 19966–19977.
8 Kijchavengkul, T.; Auras, R.; Rubino, M.; Selke, S.; Ngouajio, M.; Fernandez, R. T. Formulation selection of aliphatic aromatic biodegradable polyester film exposed to UV/solar radiation. *Polym. Degrad. Stabil*. **2011**, *96*, 1919–1926.
9 Kleemann, K.; Jaggi, M.; Bernasconi, S. M.; Schmitz, R. A.; Künkel, A.; Simon, C.; Mcneill, K.; Battagliarin, G.; Sander, M. Photochemical chain scissions enhance polyethylene glycol biodegradability: from probabilistic modeling to experimental demonstration. *Environ. Sci. Technol.* **2025**, *59*, 17773–17784.
10 Tang, D.; Zhang, C.; Weng, Y. Effect of multi-functional epoxy chain extender on the weathering resistance performance of poly(butylene adipate-*co*-terephthalate) (PBAT). *Polym. Test.* **2021**, *99*, 107204.
11 Zhang, T.; Han, W.; Zhang, C.; Weng, Y. Effect of chain extender and light stabilizer on the weathering resistance of PBAT/PLA blend films prepared by extrusion blowing. *Polym. Degrad. Stabil.* **2021**, *183*, 109455.
12 Cosate De Andrade, M. F.; Loureiro, H. C.; Sarantopóulos, C. I. G. D.; Morales, A. R. Blends of poly(butylene adipate-*co*-terephthalate) and thermoplastic whey protein isolate: a compatibilization Study. *J. Polym. Environ.* **2021**, *29*, 3288–3301.
13 Qiu, S.; Zhou, Y.; Waterhouse, G. I. N.; Gong, R.; Xie, J.; Zhang, K.; Xu, J. Optimizing interfacial adhesion in PBAT/PLA nanocomposite for biodegradable packaging films. *Food Chem*. **2021**, *334*, 127487.
14 Wang, Y.; Xu, J.; Guo, B. *In situ* constructing highly aligned ribbon-like PHBV lamellae in PBAT: towards strong, ductile and high-barrier PBAT/PHBV films. *Materials* **2025**, *18*, 3947.
15 Yan, X.; Huang, S.; Huan, J.; Li, J.; Li, X.; Wang, S.; Li, H.; Guo, X.; Ren, J.; Tu, Y. Chemical recycling of poly(butylene terephthalate) into value-added biodegradable poly(butylene adipate-*co*-terephthalate). *Polym. Chem.* **2024**, *15*, 2047–2054.
16 Liu, C.; Liu, F.; Yang, T.; Chen, C.; Lin, Y.; Wang, J.; Zhu, J. Incorporation of lactyl unit to PBAT for enhanced gas barrier property and biodegradability by direct polycondensation *via* alcoholysis of cyclic anhydride with lactic acid. *Polymer* **2024**, *313*, 127758.
17 Fan, R.; Li, B.; Liu, Q.; Liu, Q.; Cui, J.; Bai, R.; Wang, Y.; Elias, R.; Li, C.;

Graphical Abstract

Photostabilization of Poly(Butylene Adipate-*co*-terephthalate) (PBAT) Films with Hindered Amine Light Stabilizers: Performance Evaluation and Mechanistic Insights

Yang Wang, Wen-Qing He, Su-Nan Tian, Yue Wang, Run-Hao Bai, Aurore Richel, Qiu-Yun Liu, Jia-Lei Liu, Cai-Bin Li, He-Qing Cai, Zhi-Chao Zheng, and Qi Liu

Institute of Environment and Sustainable Development in Agriculture, Chinese Academy of Agricultural Sciences, China; Institute of Western Agricultural, Chinese Academy of Agricultural Sciences, China; IMDEA Materials Institute, Spain; University of Liege, Belgium; Bangor University, UK; Bijie Tobacco Company of Guizhou Province, China; Institute of Physics and Chemistry, Chinese Academy of Sciences, China

This study clarifies how different hindered amine light stabilizer (HALS) structures influence PBAT's weather resistance *via* combined structural characterizations and performance change analysis, proposes a rapid method for predicting HALS performance, and provides new ideas for the rational selection of HALS.

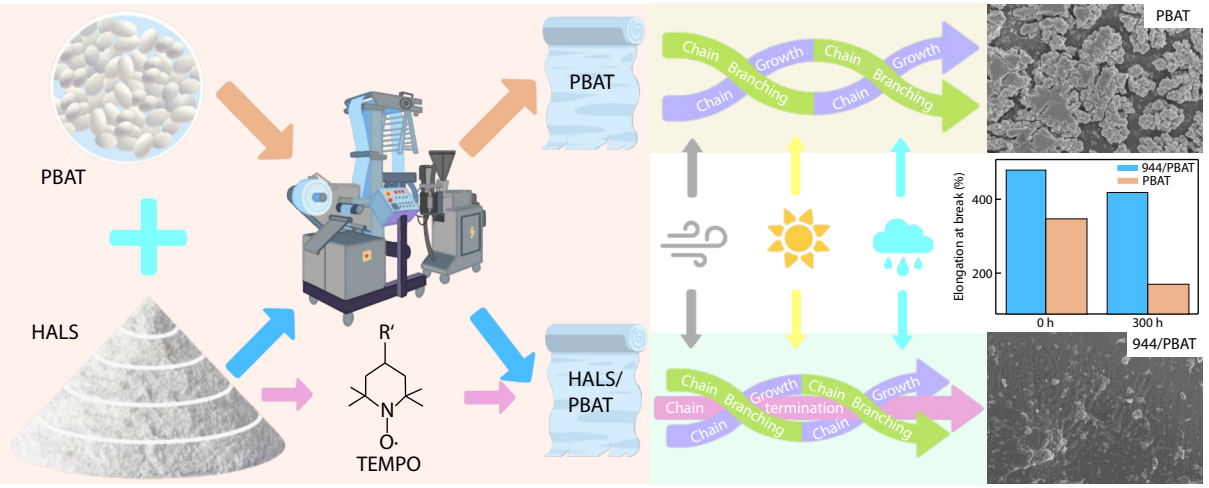

Chinese J. Polym. Sci., 2026 *https://doi.org/10.1007/s10118-026-3554-4*

He, W. Comparative evaluation of soil accumulation of light stabilizers from biodegradable mulching films versus conventional polyethylene ones. *J. Hazard. Mater.* **2024**, *465*, 133302.

18 Ma, R.; Zhao, M.; Mo, Y.; Tang, P.; Feng, Y.; Li, D. HALS intercalated layered double hydroxides as an efficient light stabilizer for polypropylene. *Appl. Clay Sci.* **2019**, *180*, 105196.

19 Deng, Q.; He, B.; Shen, M.; Ge, J.; Du, B.; Zeng, L. First evidence of hindered amine light stabilizers as abundant, ubiquitous, emerging pollutants in dust and air particles: a new concern for human health. *Environ. Sci. Technol.* **2024**, *58*, 1349−1358.

20 Souza, P. M. S.; Morales, A. R.; Sanchez, E. M. S.; Mei, L. H. I. Study of PBAT photostabilization with ultraviolet absorber in combination with hindered amine light stabilizer and vitamin E, aiming mulching film application. *J. Polym. Environ.* **2018**, *26*, 3422−3436.

21 Cho, J.; Kim, S.; Chang, I.; Kim, K.; Hong, J. Photostabilization and cure kinetics of UV-curable optical resins containing photostabilizers. *Macromol. Res.* **2007**, *15*, 560−564.

22 Davand, R.; Rahimpour, M. R.; Hassanajili, S.; Rashedi, R. Theoretical and experimental assessment of UV resistance of high-density polyethylene: Screening and optimization of hindered amine light stabilizers. *J. Appl. Polym. Sci.* **2021**, *138*, 51262.

23 Jiang, T.; Zhang, J. Comparison of UV resistance of HDPE added with hindered amine light stabilizers with different molecular structures. *Polym. Adv. Technol.* **2021**, *32*, 1288−1300.

24 Chai, R.; Chen, S.; Zhang, J. Synergistic effect of hindered amine light stabilizers/ultraviolet absorbers on the plasticized PVC during photo-irradiation. *J. Appl. Polym. Sci.* **2012**, *125*, 3376−3384.

25 Wang, X.; Pan, H.; Jia, S.; Lu, Z.; Han, L.; Zhang, H. Mechanical properties, thermal behavior, miscibility and light stability of the poly(butylene adipate-*co*-terephthalate)/poly(propylene carbonate)/polylactide mulch films. *Polym. Bull.* **2023**, *80*, 2485−2501.

26 Souza, P. M. S.; Coelho, F. M.; Sommaggio, L. R. D.; Marin-Morales, M. A.; Morales, A. R. Disintegration and biodegradation in soil of PBAT mulch films: influence of the stabilization systems based on carbon black/hindered amine light stabilizer and carbon black/vitamin E. *J. Polym. Environ.* **2019**, *27*, 1584−1594.

27 Akhir, M. A. M.; Ramakrishnan, S.; Mariatti, M. Anti-hydrolysis, UV absorber, and photostabilizer additives effect on degradation of poly(butylene adipate-*co*-terephthalate) biocomposite film for mulching application. *Polym. Adv. Technol.* **2025**, *36*, e70266.

28 Ding, Y.; Zhang, C.; Luo, C.; Chen, Y.; Zhou, Y.; Yao, B.; Dong, L.;

Du, X.; Ji, J. Effect of talc and diatomite on compatible, morphological, and mechanical behavior of PLA/PBAT blends. *e-Polymers* **2021**, *21*, 234–243.
29 ISO 4593:1993, Plastics—Film and sheeting—determination of thickness. International Organization For Standardization, **1993**.
30 Hashmi, M. S. J.; Singh, R.; Li, G.; Sharma, S.; Majumdar, G.; Hasanuzzaman, M.; Hashmi, M. S. J.; Chow, W. S.; Wahab, M. A. in *Encyclopedia of materials: Plastics and Polymers*. Elsevier, **2022**, p. 237–248.
31 Fu, Y.; Wu, G.; Bian, X.; Zeng, J.; Weng, Y. Biodegradation behavior of poly(butylene adipate-*co*-terephthalate) (PBAT), poly(lactic acid) (PLA), and their blend in freshwater with sediment. *Molecules* **2020**, *25*, 3946.
32 Kijchavengkul, T.; Auras, R.; Rubino, M.; Alvarado, E.; Camacho Montero, J. R.; Rosales, J. M. Atmospheric and soil degradation of aliphatic–aromatic polyester films. *Polym. Degrad. Stabil*. **2010**, *95*, 99–107.
33 Tabankia, M. H.; Gardette, J. Photo-chemical degradation of polybutyleneterephthalate: Part 1—Photo-oxidation and photolysis at long wavelengths. *Polym. Degrad. Stabil*. **1986**, *14*, 351–365.
34 Hodgson, J. L.; Coote, M. L. Clarifying the mechanism of the denisov cycle: how do hindered amine light stabilizers protect polymer coatings from photo-oxidative degradation. *Macromolecules* **2010**, *43*, 4573–4583.
35 Qiao, R.; Wang, X.; Qin, G.; Liu, Q.; Liu, J.; He, W. Preparation of organic crystal seed and its application in improving the functional period of biodegradable agricultural film. *Crystals* **2021**, 11.
36 Wang, J. H.; Tian, Y.; Zhou, B. Degradation and stabilization of poly(butylene adipate-*co*-terephthalate)/polyhydroxyalkanoate biodegradable mulch films under different aging tests. *J. Polym. Environ.* **2022**, *30*, 1366–1379.
37 Li, J.; Lai, L.; Wu, L.; Severtson, S. J.; Wang, W. Enhancement of water vapor barrier properties of biodegradable poly(butylene adipate-*co*-terephthalate) films with highly oriented organomontmorillonite. *ACS Sustainable Chem. Eng.* **2018**, *6*, 6654–6662.
38 Zhou, Y.; Qiu, S.; Waterhouse, G. I. N.; Zhang, K.; Xu, J. Enhancing the properties of PBAT/PLA composites with novel phosphorus-based ionic liquid compatibilizers. *Mater. Today Commun*. **2021**, *27*, 102407.
39 Hullihen, K. Determining gel content of polyethylene using a differential scanning calorimeter. *Ind. Eng. Chem. Res.* **2006**, *45*, 6095–6098.
40 Kijchavengkul, T.; Auras, R.; Rubino, M. Measuring gel content of aromatic polyesters using FTIR spectrophotometry and DSC. *Polym. Test*. **2008**, *27*, 55–60.
41 Da Silva, J. R. M. B.; Cavalcanti, R. S. F. B.; Rabello, M. S. Chemical degradation and failure analyses by acoustic emission of PP/EOC blends exposed to ultraviolet radiation. *Polym. Eng. Sci*. **2020**, *60*, 3135–3148.

https://doi.org/10.1007/s10118-026-3554-4